Effect of surfactant lengths on gas-liquid oxygen mass transfer from a single rising bubble

Gaëlle Lebrun, Sanae Benaissa, Claude Le Men, Véronique Pimienta, Gilles Hébrard, N. Dietrich

Effect of surfactant lengths on gas-liquid oxygen mass transfer from a single rising bubble

Gaëlle Lebrun[1], Sanae Benaissa[1], Claude Le Men[1], Véronique Pimienta[2], Gilles Hébrard[1], Nicolas Dietrich[1,*]

[1] Toulouse Biotechnology Institute (TBI), Université de Toulouse, CNRS, INRAE, INSA, Toulouse, France

[2] Laboratoire des IMRCP, Université de Toulouse, CNRS UMR 5623, Université Paul Sabatier, Toulouse, France

*Corresponding author: dietrich@insa-toulouse.fr (N. Dietrich)

Abstract

This work is an experimental investigation of the effect of the nature of surfactants on oxygen mass transfer. The study focuses on three cationic surfactants with different hydrophobic chain lengths, and four nonionic surfactants with different hydrophilic chain lengths. Equilibrium adsorption isotherms are calculated for each surfactant from experimental values of surface tension in static conditions. Surfactant solutions at concentrations between 2.5×10^{-8} and 5×10^{-3} mol/L were prepared and oxygen transfer from millimetric air bubbles (between 0.82 and 1.08 mm) was measured by Planar Laser Induced Fluorescence with Inhibition (PLIF-I). When the bulk concentration of surfactant was increased, results showed a sharp decrease of bubble velocity, in the range of 283 – 75 mm/s, and of liquid-side mass transfer coefficient, in the range of 5.6×10^{-4} - 0.4×10^{-4} m/s. This effect was observed for all surfactants studied. However, the length of the hydrophilic chain did not appear to affect the hydrodynamics of the rising bubble or the oxygen transfer at the same bulk concentration. Furthermore, for the same bulk concentration, increasing the hydrophobic chain length had an impact on the velocity and the mass transfer coefficient of oxygen. Finally, the Sherwood number was calculated in each medium and compared with classical correlations for gas-liquid mass transfer prediction. Those correlations seemed to reach a limit for a very concentrated medium.

Keywords

Surfactants, Oxygen mass transfer, Bubble, PLIF-I, adsorption

1. Introduction

Gas/liquid systems involving mass transfer occur in numerous chemical, biochemical or environmental processes [1-4]. Among these, wastewater treatment plants using activated sludge tanks are at the core of process intensification for oxygen mass transfer. The oxygen mass transfer coefficient is a key parameter to optimize the process because oxygen is used to keep pollutant-degrading bacteria alive, so a good prediction of the mass transfer coefficient is required to enable the process to be adjusted toward a decrease of power consumption for the same performance. Seeing this strong industrial demand, intensive studies have been carried out to investigate the global mass transfer in gas-liquid contactors [5–8]. For two decades, studies have been oriented toward hydrodynamics and contactors at a more local scale but, for good comprehension of all the phenomena occurring in bubble columns, the molecular, bubble and laboratory scales have to be taken into account [9].

The physicochemical properties of the liquid phase can affect the hydrodynamics and mass transfer in a column and some studies have focused their research on viscous media [10,11] or media close to the one found in aerated sludge tanks with the coupled effect of rheology and surface tension [12–14]. The effect of the surface tension on mass transfer has also been largely studied. Surfactants come from all kinds of domestic detergents and, due to their amphiphilic properties, they adsorb on the gas/liquid interface, influencing hydrodynamics and mass transfer. They are considered as the most common contaminants hindering oxygen transfer [15,16] but the mechanisms explaining this decrease are still under debate. Various authors have identified a decrease that occurs because of hydrodynamic modifications brought by surfactants, such as an increase of interfacial rigidity that decreases the renewal rates close to the bubble and decreases its terminal velocity [17–21] or a modification of the velocity field surrounding the bubble [22], and also physicochemical modifications [23–25]. Although

the decrease of mass transfer and velocity is widely reported in the literature, Gómez-Díaz et al. underlined the increase of mass transfer coefficient appearing with the addition of a very weak concentration of cationic surfactant. This increase was attributed to greater gas/liquid interfacial buoyancy due to the Marangoni effect [26], an effect also identified later by Alvarez et al. with an anionic surfactant [27]. In their studies, Painmanakul et al. (2005) and Sardeing et al. (2006) highlight the link between the mass transfer coefficient, the diameter of the bubbles and the surface coverage by surfactants [28,29].

In addition, the surface properties of amphiphilic molecules depend on their structure, so they affect mass transfer in different ways. It has been observed that the charge of the head [23,30–34] or the length of the tail [21,35] largely affects mass transfer, since these parameters affect the affinity of surfactants with the interface. However, although these parameters have been studied, to the best of our knowledge, no general conclusion can be drawn about the influence of the surfactant's nature.

Mass transfer in presence of surfactants seems to involve very complex mechanisms and some research has focused on studying the numerical resolution of these complex systems. Some authors use direct numerical simulation (DNS) to predict the local distribution of surfactants around a bubble, and thus gain a better understanding of hydrodynamic and physicochemical phenomena close to the interface, which is promising for mass transfer models [36,37] . In addition, for a better understanding of local phenomena, a few techniques for direct visualization of mass transfer have been developed. This is the case of Laser Induced Fluorescence methods (LIF) which use a pH sensitive dye to visualize gas/liquid transfer of CO_2 in clean or contaminated media [13,38–44]. Another visualization technique uses the properties of fluorescence inhibition by a quencher. This is the case of Planar Laser Induced Fluorescence with Inhibition (PLIF-I) to measure oxygen transfer, which uses a fluorescent dye that is inhibited in the presence of oxygen and can measure oxygen transfer in different geometries, such as plane interfaces [45–47] Taylor bubbles [48–51], and bubble columns [22,52,53].

The present work focuses on the measurement of oxygen transfer from isolated millimetric air bubbles in media containing various surfactants of different, accurately-chosen natures. To achieve this goal,

the technique of PLIF-I presented above was used. Cationic and nonionic surfactants were used and were chosen because of their similar global structures but different lengths of the hydrophobic or hydrophilic part. First, an in-depth study of interface colonization by these surfactants was performed. Then mass transfer was studied for different concentrations of each surfactant, the objective being to highlight the link between the chemical structure of the surfactant, its interface colonization and gas/liquid oxygen transfer.

2. Material and methods

2.1. Oxygen transfer measurements

Planar Laser Induced Fluorescence with Inhibition (PLIF-I) was used in this study to quantify the oxygen transfer and hydrodynamic parameters of the bubble in different media. The experimental setup is represented in Figure 1. It is composed of a column (1) (10x10x30 cm^3) filled with the solution. A 75 µm internal diameter needle connected to a syringe pump, which can be activated remotely (Harvard apparatus PHD, 22/2000 Programmable, USA) (2), generates single air bubble. A CMOS camera (3) (12 bits, 1920x1200 $pixel^2$, Basler ace, Germany) placed next to the column, 50 mm above the injection point, can record 250 images/s in a window of 1920x500 $pixel^2$ at 20.31±0.04 µm/pixel. This camera was positioned in such a way as to measure the surface area and velocity of the bubble; the viewing window was then around 39x10 mm^2 (the highest visualization axis on the vertical direction). The backlight used was a white LED (100x100 LLUB, PHLOX, France). The geometrical calibration of the camera was performed with a precision rule and concerning the uncertainty of this method it is calculated as the thickness of one graduation bar. Then, the velocity is calculated with the time taken by the bubble to cross the 39 mm window, and the size of the bubble by a binarization of the bubble images and contour analysis (see figure 1).

The amount of oxygen transferred in the wake of the bubble was measured by fluorescence inhibition of a ruthenium complex (CAS: 20782-45-7, Sigma-Aldrich, USA), which was excited by a horizontal laser sheet (4) (Nd:YAG, laser: Dualpower 200-15, 15Hz, 2x200 mJ, Dantec Dynamics, Denmark) at 532 nm, in a plane perpendicular to the bubble wake, 50 mm above the injection plane. Fluorescence

intensity was recorded by a CCD camera (5) (FlowSense, 12 bits, 2048x2048 pixels, Dantec Dynamics, Denmark). This camera was placed at the bottom of the column with a sampling of 4.37±0.04 μm/pixel (viewing window about 9x9 mm^2), focused on the laser sheet. It was equipped with a 570 nm high pass filter in order to record only the fluorescence from the ruthenium complex, which has an emission wavelength of 582 nm. The camera speed was synchronized with the laser frequency and focused on the laser sheet. Before each experiment, a calibration curve was built by using an oxygen probe (multimeter: HQ40D, probe: Intellical LDO101, Hach, Germany) to associate each grey level with an oxygen concentration, according to the Stern Volmer [54] equation (1)

$$1/G=1/G_0+K_{sv}/G_0 \times [O_2] \quad (1)$$

where G is the grey level, G_0 is the grey level in absence of the quencher, $[O_2]$ mg/L is the oxygen concentration and K_{sv} is the Stern Volmer constant. Once the calibration curve was applied to the images obtained in the bubble wake, the oxygen concentration was displayed on each pixel. To calculate a mass transfer coefficient from experimental data, a threshold criterion was verified according to equation (2), where I is the maximal intensity of the signal, I_0 the intensity of the background, and σ_n the standard deviation of the background (square root of the expected value of the squared deviation from the mean). The signal was considered as significant if the signal-to-noise ratio was higher than 10.

$$(I-I_0)/\sigma_n>10 \quad (2)$$

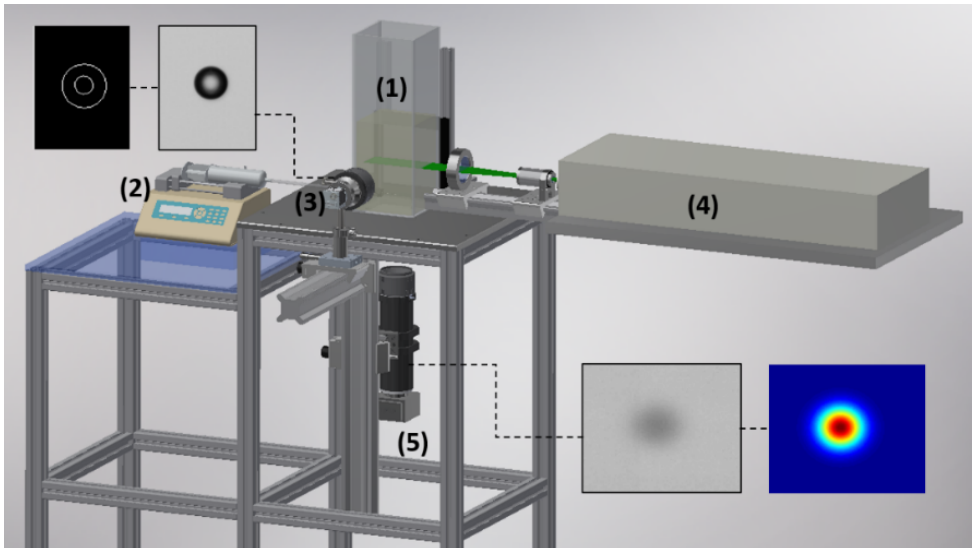

Figure 1: Experimental setup used to measure gas/liquid oxygen transfer by PLIF-I

The second criterion to be verified was the mass conservation in the wake plane in function of time if the absence of convection was to be assumed. Figure 2 displays the integral of the spot, which represents the total mass transferred in the plane, versus time. It is constant from 0.4 to 2.4 seconds, with a small standard deviation. The average of these values gave the total mass transferred in a plane perpendicular to the bubble wake. After 2.4 seconds, the noise was too great to allow an accurate integral to be calculated and, finally, the criterion described by equation (2) was no longer valid.

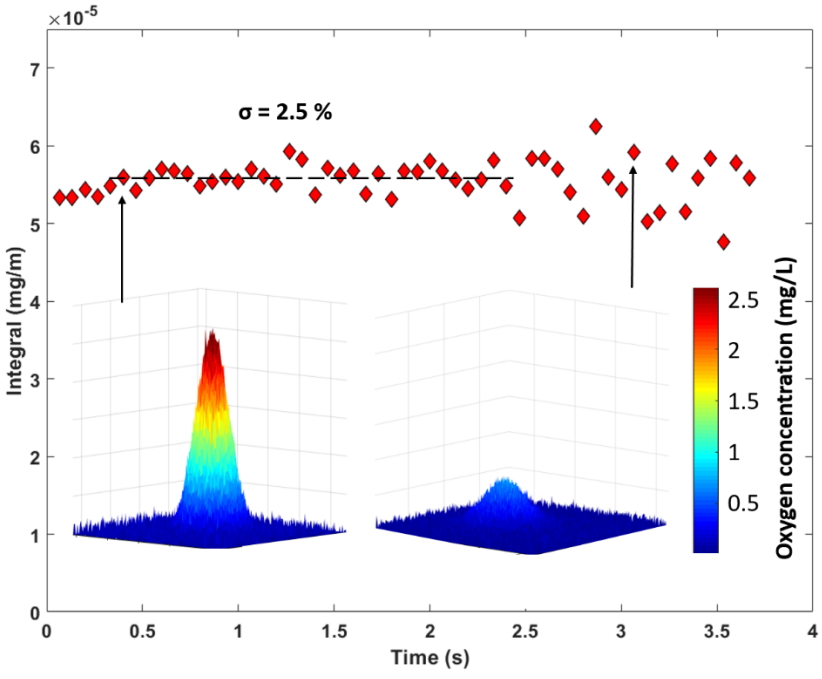

Figure 2: Integration of the oxygen field concentration in the wake of the bubble with time

Once these criteria had been verified, it was considered that the mass transferred in a horizontal plane was constant and the change in the size of this spot structure was thus due solely to molecular diffusion of oxygen. In previous studies [52,55,56], it was observed that, for quasi-spherical bubbles, the diffusion spot was circular and presented a Gaussian profile. As a result, the diffusion spot was fitted by equation (3), where the concentration $[O_2]$ in each pixel x_p, y_p was estimated.

$$[O_2](x,y)=A\times\exp((-(x_p-X)^2+(y_p-Y)^2)/B+C) \quad (3)$$

Parameters were found by fitting the equation with the raw image using the "fminsearch" solver (Matlab R2017a). Note that A and B are parameters, and (X, Y) is the centre of the spot, the parameter C representing the background.

It was possible to calculate the flux of oxygen (mg/s) transferred by the rising bubble with equation (4), where V_b is the velocity of the bubble (m/s) measured by the side camera.

$$F_{O2}=V_b\times\iint[O_2](x,y)dxdy \quad (4)$$

The mass transfer coefficient was then deduced from equation (5), where S_b is the surface area of the bubble, deduced from the equivalent diameter measured with the side camera; $[O_2]$ is considered as the concentration at the beginning of the experiment (measured with the optical oxygen probe, close to 0 mg/L); and $[O_2]^*$ is the saturation concentration of oxygen, measured by the optical oxygen probe.

$$k_L=F_{O2}/(S_b\times([O_2]^*-[O_2])) \quad (5)$$

Finally the diffusion coefficient of oxygen in the bulk was measured by a method developed by Xu et al. [57] assuming that the surface area of the spot S_{spot} increased with time following equation (6)

$$S_{spot}=2\pi D_{O2}t\eta_D \quad (6)$$

where η_D is a constant that can be fixed following the procedure described by Xu et al. [57]. Then the surface area of the spot was plotted versus time and the diffusion coefficient was extracted from the slope.

Each condition was repeated 6 times in order to be sure of the repeatability of measurements. All measurements were performed at room temperature (294±1K).

2.2. Physicochemistry of systems studied

The surfactants used were cationic or nonionic. They are presented in Table 1. The three cationic surfactants were hexadecyltrimethylammonium chloride (C16TAC, Sigma Aldrich, CAS: 112-02-7, USA), dodecyltrimethylammonium chloride (C12TAC, Sigma Aldrich, CAS: 112-00-5, USA) and trimethyloctylammonium chloride (C8TAC, Sigma Aldrich, CAS: 10108-86-8, USA) with respectively 16, 12 and 8 carbons on their linear carbonated chain. They shared the same, positively charged, hydrophilic head: an ammonium chloride. Concerning nonionic surfactants, experiments were run with Triton X-100 (TX100, CAS: 9002-93-1, Sigma Aldrich, USA), Triton X-102 (TX102, CAS: 9036-19-5, Sigma Aldrich, USA) and Triton X-165 (TX165, CAS: 9636-19-5, Sigma Aldrich, USA) and TX305 (CAS: 9002-93-1, Sigma Aldrich, USA). These nonionic surfactants present the same hydrophobic structure and a hydrophilic polyethylene oxide chain with a different average number of repetitions; 9.5, 12, 16 and 30 for TX100, TX102, TX165 and TX305 respectively. All surfactant solutions were prepared with ultra-pure water (18 mΩ/cm).

Surfactant	Type	Molecular formula	n	Molar mass (g/mol)	CMC (mmol/L)	HLB (without unit)
C_8TAC	cationic	$CH_3(CH_2)_nN(CH_3)_3Cl$	7	208	320	12.7
C_{12}TAC			11	264	6	10.8
C_{16}TAC			15	320	0.8	8.9

TX100	nonionic	t-oct-C_6H_4-$(OCH_2CH_2)_nOH$	9.5	624	0.30	13.4
TX102			12	734	0.36	14.4
TX165			16	910	0.62	15.5
TX305			30	1526	1.3	17.3

Table 1: Information on the surfactants used in the study

The mass transfer coefficient was measured in solutions presenting concentrations between $2.5x10^{-8}$ mol/L and $5x10^{-3}$ mol/L. The equilibrium surface tension was measured for each solution with the Nouÿ ring method (tensiometer: K6, Krüss, Germany), assuming that equilibrium surface tension was reached after 2 hours [31]. To be sure of the repeatability of the measurements, each point was repeated 6 times and the deviation was lower than the error predicted by the supplier (1 mN/m). The surface tension was linked to the surface concentration; this effect is described by the Gibbs equation (7) [58].

$$\Gamma=-nRT\ln(d\gamma/dC) \quad (7)$$

where Γ is the surface concentration (mol/m^2), n is equal to 1 for nonionic or 2 for ionic surfactants, R is the perfect gas constant (J.mol^{-1}K^{-1}), T the temperature (K), γ the surface tension (N/m) and C the bulk concentration (mol/m^3). The Gibbs equation comes from a thermodynamic description of the system and, to access the surface concentration, adsorption models are more commonly used. In this study, the Langmuir model [59] was used for the nonionic surfactants, and is described by equation (8)

$$\Gamma=\Gamma_{max}\times K_{LG}\times C/(1+ K_{LG}\times C) \quad (8)$$

where Γ_{max} is the maximal surface concentration (mol/m^2), and K_{LG} is the Langmuir constant (m^3/mol). Concerning the cationic surfactants, the Langmuir model is not the most suitable since it assumes that there is no interaction between monomers. For this kind of surfactants, the Frumkin model [60] is more useful because it takes electrostatic interactions between molecules into account. The model is described by equations (9) and (10)

$$\gamma=\gamma_0+(R\times T\times \Gamma_{max})\times[\ln(1-\theta)+a\times\theta^2] \quad (9)$$

$$K_F\times C=\theta/(1-\theta)\times\exp(-2\times a\times\theta) \quad (10)$$

where K_F is the Frumkin constant (m^3/mol), θ is the degree of coverage by the surfactant, given by $\theta=\Gamma/\Gamma_{max}$, and a is a constant accounting for intermolecular interactions. Both models were solved numerically to fit the experimental points. The numerical resolution was performed by a free access software "Sa" (http://cinet.chim.pagesperso-orange.fr/tele_sa/install_Sa_Eng.html).

The critical micellar concentration (CMC) given by Table 1 was extracted from the curves of surface tension according to the bulk concentration. Details of this value will be given in the next section. Concerning the Hydrophilic Lipophilic Balance (HLB), the values were provided by the supplier for nonionic surfactants and calculated from the Davies formula [61] for cationic surfactants. The HLB is a scale representing the affinity of the surfactant with the different phases. The higher the HLB, the more hydrophilic the surfactant and, thus, the greater its affinity with water. That is why, in the table, HLB is observed to decrease when the hydrophobic part of a cationic surfactant increases, and HLB increases when the hydrophilic part of the nonionic surfactants increases.

In order to confirm that surfactants did not affect the rheology of the solution, viscosity was measured for shear rates between 1 and 500 s^{-1} with a rheometer (HAAKE MARS III, Germany). For all surfactants in the range of concentrations of the study, the viscosity was found to be the same as that of water (1.00±0.07 mPa.s).

Finally, mass transfer experiments were also tried with anionic surfactants. However, due to their negative charge, which is opposite to the positive charge of the ruthenium complex, interaction between the two created a complex that settled in the solution. This complex made measurement by PLIF-I impossible. As far as we know, no fluorescent dye has been used for measuring oxygen transfer in presence of an anionic molecule.

3. Results and discussion

3.1. Study of the interface colonization

Surfactants were selected for this study because they present different structures and, as a result, may have different ways of colonizing the interface. This part deals with the equilibrium state of interfaces with chosen surfactants. To characterize interfaces in presence of surfactants, a key parameter is the surface tension. Figure 3 A and B present the equilibrium surface tension according to the bulk concentration for all of the surfactants studied.

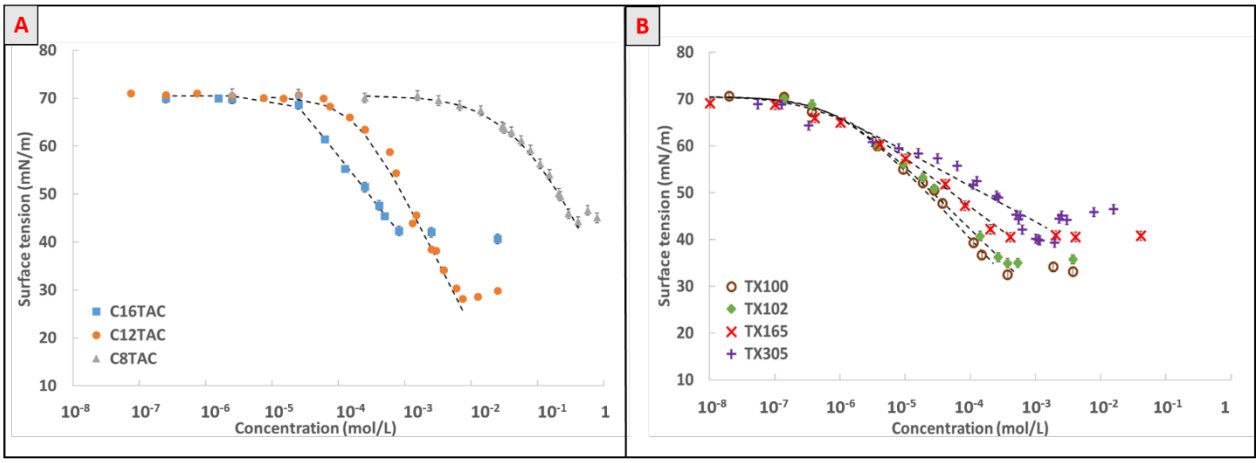

Figure 3: Equilibrium surface tension of surfactant solutions according to bulk concentration. A: cationic surfactants (dotted lines represent surface tension modelled by Frumkin). B: nonionic surfactants.

Each curve is representative of a classical surfactant behavior. (i) At low concentration, the surface tension is equal to the surface tension of water, so no – or a negligible amount of – surfactant is adsorbed. (ii) A sharp decrease in surface tension occurs with increasing concentration, corresponding to a gradual adsorption of surfactant on the interface. (iii) At high concentration, from a value called the critical micellar concentration (CMC), the surface tension becomes constant: the system is no longer considered as diluted, the surfactant aggregates in the form of micelles, and the interface has reached its maximal surface concentration in the pressure and temperature conditions considered.

Even though the surfactants present the same classical curve shape, some differences can be noticed at this stage of the study. First, increasing the hydrophobic chain length of cationic surfactant leads to a large change in the value of the CMC, and the decrease of surface tension does not take place for the same bulk concentration. We expected these surfactants to reach approximately the same value of surface tension after the CMC, as is usually reported in the literature [62,63]. This was the case for C16TAC and C8TAC, which reached a value close to 43 mN/m. However, for C12TAC, the measured value was around 10 mN/m weaker. This can be attributed to an impurity in the product, which was used as received from the supplier. The impurity may have been the corresponding long chain alcohol [64]. The behavior is different if the hydrophilic chains of nonionic surfactants are lengthened as the change in both the CMC value and the surface tension value above the CMC is very small. These 7 curves were used to calculate the equilibrium surface concentration since the systems were solved numerically, the dotted lines of Figure 3 representing the model that best fits the experimental points of surface tension. Table 2 and Table 3 present the parameters obtained for cationic and nonionic surfactants respectively.

	C8TAC	C12TAC	C16TAC
K_F (m^3.mol)	0.02	2.58	3.38
a (without unit)	0.04	0.63	2.75
Γ_{max} (mol.m^{-2})	2.43×10^{-6}	2.48×10^{-6}	1.54×10^{-6}

Table 2 : Adsorption parameters obtained by using Frumkin model for cationic surfactants

	TX100	TX102	TX165	TX305
K_{LG} (m^3.mol)	1053	1194	2440	3294
Γ_{max} (mol.m^{-2})	2.67×10^{-6}	2.43×10^{-6}	1.90×10^{-6}	1.36×10^{-6}

Table 3 : Adsorption parameters obtained by using Langmuir model for nonionic surfactants

From these fitted parameters, values of equilibrium surface concentrations according to bulk concentrations are presented in Figure 4 A and B for each surfactant studied. From Table 2, Table 3,

and Figure 4, regarding the maximal surface concentrations (Γ_{max}), the longer the chain is, the lower is the maximal surface concentration. This tendency was observed for nonionic surfactant and cationic surfactant, even though C8TAC and C12TAC reached a very close maximal surface concentration. This can be attributed to the impurity discussed above in this section. However, although this effect is verified for each kind of surfactant, it does not hold true between the two different kinds of surfactants: even though the nonionic surfactants present a bigger molar mass than the cationic ones, their maximal interfacial concentrations are higher or very close. The parameter a is higher for the longest chains, but decreases and is almost negligible for C8TAC. This means that the molecular interactions are important for the longest chains but do not play an important role for the shortest chain and the Frumkin isotherm is very close to a Langmuir isotherm. Finally, the adsorption constants of cationic surfactants increase with the length of the tail and this is consistent with the values of HLB: increasing the proportion of hydrophobic part decreases the solubility of the surfactants. Concerning the nonionic surfactants, their high adsorption gives them the same solubility properties.

In accordance with the constants K_K and K_{LG}, adsorption of nonionic surfactant took place for the same bulk concentrations for each chain length studied. In contrast, for cationic surfactants, the more hydrophilic they were, the more they adsorbed at high concentrations.

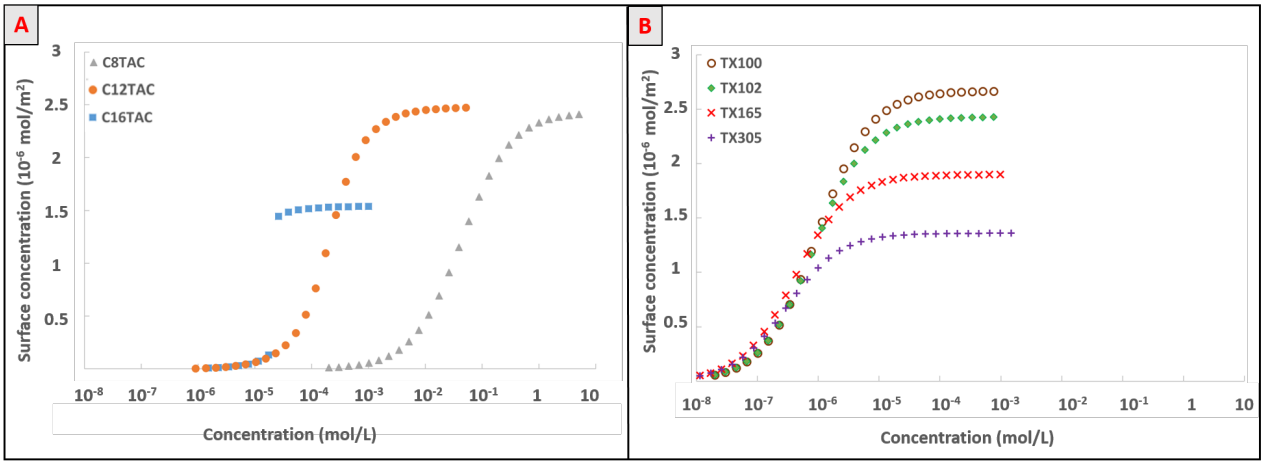

Figure 4: Molar equilibrium surface concentration of surfactants in function of bulk concentration. A. Cationic surfactants from Frumkin isotherm. B. Nonionic surfactants from Langmuir isotherm.

To view this colonization from another standpoint, it is interesting to calculate the surface concentration, not in terms of number of moles, but in mass quantity. Figure 5 A and B represent the surface concentration in grams per square meter according to the molar concentration of the bulk. The first point highlighted by this figure is the difference between the maximal surface concentrations of nonionic surfactants and cationic surfactants. The mass of triton adsorbed on the interface was around 3 times the maximal surface concentration of cationic surfactants. This time, the curves show that the longer the chain of a nonionic surfactant, the higher its maximal mass concentration: even though the maximal surface concentration of TX165 reached a value between TX102 and TX100, the tendency was more marked with the higher value of TX305. This effect was less marked for cationic surfactants, for which no trend could be noted.

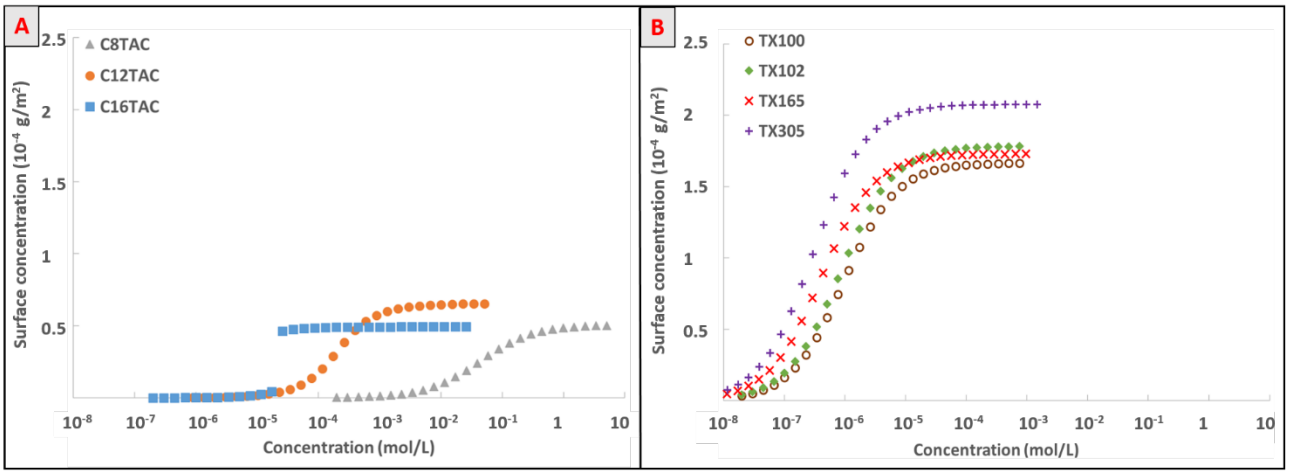

Figure 5: Mass equilibrium surface concentration of surfactants versus bulk concentration. A. Cationic surfactants from Frumkin isotherm. B. Nonionic surfactants from Langmuir isotherm.

Once the equilibrium surface colonization of surfactants had been highlighted, mass transfer measurements in the same kind of media could contribute information about the influence of the chain length, and also the affinity with the interface at different concentrations, on oxygen transfer.

3.2. Oxygen transfer in different media

The objective of this part is to highlight the effect of surfactants on oxygen transfer, comparatively to their affinity with the interface. First, the impact of the surfactant on the hydrodynamic parameters of

the bubble needs to be considered since these parameters play an important role in mass transfer. The bubble diameter varied slightly between experiments, as the presence of surfactant tends to facilitate the detachment of bubbles and lead to smaller bubbles. Nevertheless, recorded diameters were between 0.82±0.02 mm and 1.08±0.02 mm. The mean diameter of each condition can be found in the supplementary material. The velocities of bubbles were strongly impacted by the presence of surfactants. Figure 6 A and B represent the velocity according to the bulk concentration. For all surfactants studied, increasing the concentration led to a decrease in the bubble velocity. For nonionic surfactants, the curve plotting this decrease has the same shape for any chain length and reaches a plateau around 0.1 m/s. In contrast, changing the tail length of cationic surfactants led to a translation of the curve. The impact on velocity appears at high concentrations with short tail surfactants and at low concentrations with long tail surfactants. These results can be explained by differences in the concentration of surfactants adsorbed at the interface. Indeed, while nonionic surfactants are adsorbed at the interface for the same bulk concentration, the cationic surfactants are adsorbed on the interface for very different concentration in the liquid phase. For example, for a concentration in the liquid phase of 10^{-4} M, the maximal surface concentration of C16TAC is reached while C8TAC has not yet begun to colonize the interface. These differences in surface concentration lead to differences in the Marangoni force, which is opposite to the convection and responsible for the decrease in the velocity of bubbles when surfactants are present [65]. It is important to keep these bubble velocities in presence of surfactants in mind because they are used to calculate the mass transfer coefficient according to equation (4).

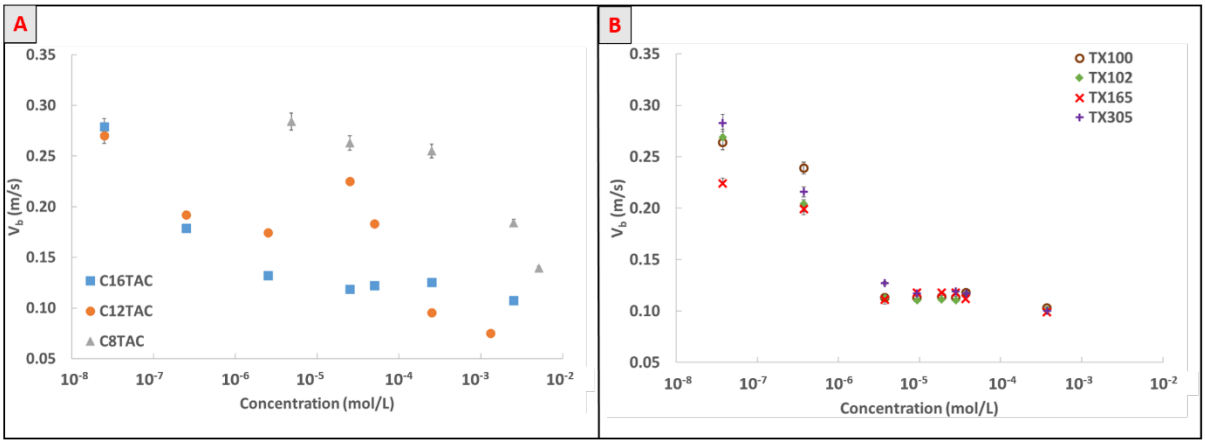

Figure 6: Velocities of bubbles according to bulk surfactant concentrations. A. Cationic surfactants. B. Nonionic surfactants

Concerning the study of oxygen transfer, Figure 7 gives examples of results obtained from PLIF-I for the TX100 series. Since the velocities of the bubbles are different, it represents different position in the tail of the bubble, however, the total mass transferred is conserved with time (see figure 2), as a results the images can be significantly compared. From these first results, it is obvious that the amount of mass transferred decreases with the increase of TX100 bulk concentration. However, the total mass transferred—in other words the integral of the spot—for the higher concentration of 3.7×10^{-4} mol/L seems to be higher than for the lower concentration of 2.8×10^{-5} mol/L. This effect does not follow the trend of the mass transfer to decrease with increasing concentrations of surfactant and stresses the importance of taking the velocity of the bubble into account. The velocity is higher for the lowest concentration and, as a result, the flux of oxygen transferred is higher even if the total mass transferred is lower. All information about important calculated parameters in each case is given in Tables 4,5,6,7,8,9 and 10, available in the supplementary material. This result was observed for each surfactant studied.

In order to compare all the results obtained for our sets of surfactants, the mass transfer coefficient was plotted against the bulk concentration of surfactants; the results are presented in Figure 8. The error bars represent the uncertainty of the measures. Since each measurement was made 6 times, the relative

standard deviation of mass transfer coefficient is given in Tables 4,5,6,7,8,9 and 10, available in the supplementary material.

For each surfactant, a decrease of mass transfer coefficient was observed with increasing concentration of surfactant. This effect is described in the literature, where it is usually associated with hydrodynamic effects on the bubble [18,22,43]: adsorption of surfactant on the bubble tends to make it more rigid and the renewal at the interface decreases, leading to a decrease of transferred flux.

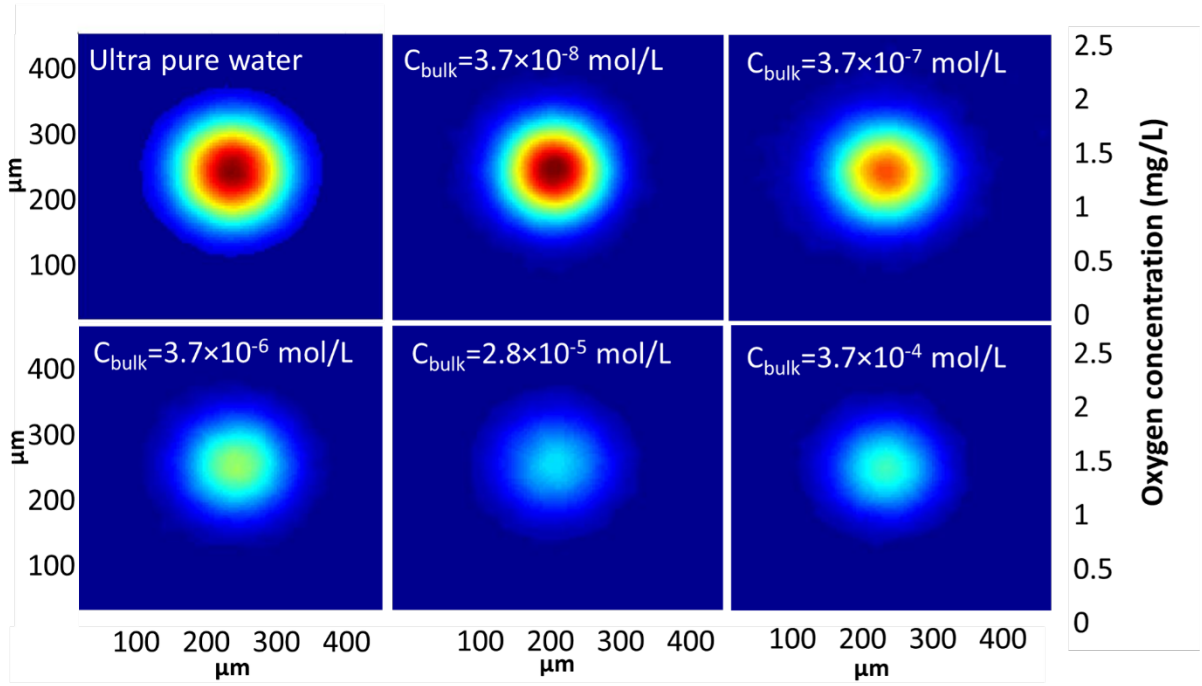

Figure 7: Oxygen concentration field in the wake of a bubble 0.33 seconds after the bubble's passage, in solutions containing different concentrations of TX100

Concerning the mass transfer coefficient related to the nature of the surfactant, once again, different behaviors can be seen in Figure 8 for the two kinds of surfactant studied. Error bars are displayed for each point although, for very concentrated solutions, the bar is smaller than the symbol itself. First of all, it is interesting to compare the curve of mass transfer coefficient with those of velocity (see Figure 6). The decrease of mass transfer coefficient is closely linked with the velocity of the bubble. The slowdown due to the presence of surfactant leads to a decrease of the surface renewal and this seems to be the major effect leading the decrease of mass transfer. The effects of surfactants on the

hydrodynamics leading to a decrease of mass transfer coefficient are described by current correlations and this point will be discussed in the next part. Concerning cationic surfactants, for the same concentration, an addition of 4 carbons on the carbonated chain leads to a different mass transfer coefficient. This decrease of mass transfer coefficient with the chain length of the same kind of surfactant has been observed by Garcia-Abuin et al. [35] in a bubble column. This information may be linked with results described part 3.1 (Figure 4 and Figure 5), because the adsorption of surfactant on the interface is translated from low concentrations for long chains to high concentration for short chains. These facts suggest that the decrease of mass transfer coefficient is linked to the equilibrium adsorption at interfaces. A similar analysis can be applied to nonionic surfactants but, this time, whatever the hydrophilic chain length, the mass transfer coefficient is the same for an identical molar concentration. Interestingly, this effect can be linked with Figure 4 and Figure 5 and, unlike the situation for cationic surfactants, the surface concentration increases for all hydrophilic chains when the bulk concentration is the same. These observations encourage us to assume that the adsorption isotherm and the surface concentration are very important parameters, and the hydrophobic chain length influences these parameters.

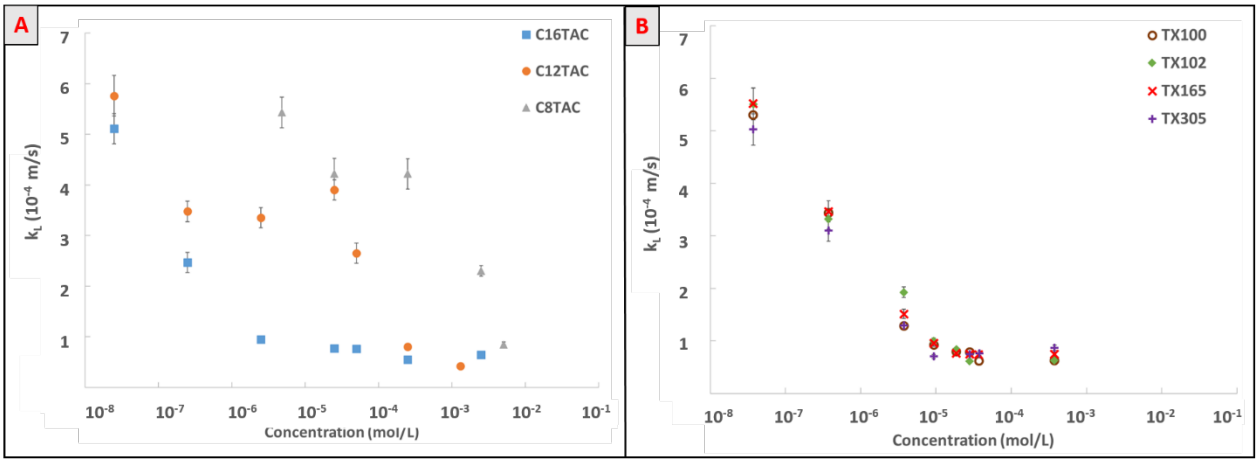

Figure 8: Mass transfer coefficient of oxygen according to bulk concentration of surfactant. A: cationic surfactants. B: Nonionic surfactants

Furthermore, the maximal surface concentrations of nonionic surfactants are different in terms of molar or mass concentration but the mass transfer coefficient reaches a plateau and stays the same for

any chain length at very high concentration. This means that the hydrophilic part of the surfactant has no effect on the mass transfer coefficient, even though it changes the interface density. It would have been interesting to have the same information on reaching a plateau for cationic surfactants in order to draw a conclusion about the effect of the hydrophobic chain length. Unfortunately, although the plateau is reached for the C16TAC, this is not the case for C12TAC and C8TAC because, for concentrations higher than 1.3×10^{-3} and 5.1×10^{-3} mol/L the signal received by the camera is too low and so not sufficient to satisfy the criterion determined by equation (2). However, we can still guess that their k_L are different from the value of the plateau for C16TAC since the signals received are lower. We assume that, unlike the hydrophilic chain length of nonionic surfactant, the hydrophobic chain length has an impact on mass transfer. However, a method to capture lower flux would be needed to confirm this assumption.

Finally, although some conclusions can be drawn about the effect of the length of the surfactant, it is important to keep in mind that adsorption is a dynamic phenomenon and some studies have highlighted the importance of adsorption kinetics, especially for its effect on the velocity of rising bubbles [66]. This means that surfactants are not immediately adsorbed on the bubble with the same concentration as described in Figure 4 and Figure 5. So a parameter that needs to be taken into consideration is the dynamics of the adsorption of surfactant on a rising bubble. From the short distance and with the window of visualization used here, this parameter is difficult to measure.

3.3. Oxygen transfer in presence of surfactants: limitation of the model

This article provides many data concerning mass transfer for bubbles that are clean, or partially or fully contaminated. These results can be compared with commonly used models for predicting mass transfer. We chose to use the Sherwood number according to equation (11) in order to nondimensionalize the calculation.

$$Sh=k_L\times d_{eq}/D_{O2} \qquad (11)$$

Figure 9 represents the Sherwood number as a function of the Reynolds number. Error bars were calculated for each point but are not visible for low Sherwood and Reynolds numbers. In order to also

represent the ratio of contamination of the bubble, every point is colored according to θ ($=\Gamma/\Gamma_{max}$). Experimental results are compared with predictions of the Higbie [67] and Frössling [68] models, which represent clean and fully contaminated bubbles, respectively, calculated with equations (12) and (13).

$$Sh_{Higbie}=1.13\times Re^{0.5}\times Sc^{0.5} \quad (12)$$

$$Sh_{Frössling}=2+0.66\times Re^{0.5}\times Sc^{0.33} \quad (13)$$

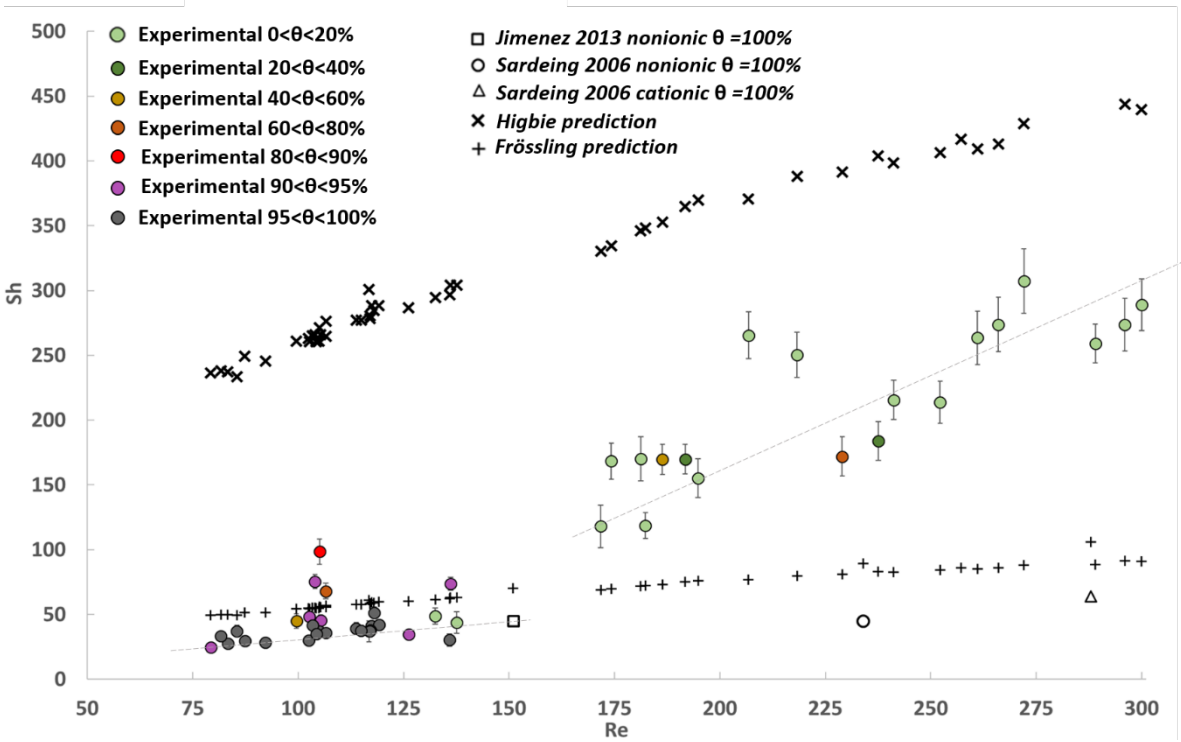

Figure 9: For cationic and nonionic surfactants with different coverage ratios, Sherwood number as a function of Reynolds number.

Some interesting information can be obtained from this figure. First, the Reynolds number is strongly impacted by the increasing coverage ratio. As predicted in the literature [69], the presence of surfactants leads to a decrease of velocity and bubble diameter; these parameters are taken into account with the Reynolds number. Secondly, a sharp decrease of the Sherwood number is observed with a decrease of the Reynolds number and an increase of the coverage ratio. This decrease of Sherwood number can be described with two different slopes (represented by dotted lines on Figure

9). The first, for high Reynolds numbers, is the steepest. The equilibrium contamination of bubbles is weak and even a slight increase leads to a marked decrease in the Sherwood and Reynolds numbers. As expected, the value of Sherwood numbers in this first slope are found to lie between the values predicted by Frössling and by Higbie. The same trend has been observed by Sardeing et al. for low surface coverage [29]. The second slope is for low Reynolds number and high level of contamination. The slope is slight but the surprising result is that the Sherwood numbers are lower than those predicted by Frössling for all the bubbles with a coverage ratio between 95 and 100%, and for a large majority of bubbles with a coverage ratio higher than 90%. This result shows the limits of the Frössling model for highly contaminated bubbles. This overestimation can be as high as 50% for very concentrated solutions, which is not negligible and cannot be attributed to experimental errors. Similar results have already been observed by Jimenez (2013) [70] with monoglyceride caprylate as nonionic surfactant, and by Sardeing et al. for high surface coverage [29] with Lauryl dimethyl benzyl as cationic surfactant and a fatty alcohol as nonionic surfactant. These two previous studies measured the transfer for bigger bubbles, with diameters between 1.2 and 1.6 mm, which led to higher Reynolds numbers than the ones calculated in this study. The calculated Sherwood numbers are presented in Figure 9 and overestimation by the Frössling model is observed. These results highlight the necessity to introduce a correction into the Frössling model for very highly concentrated bulk. It is most likely that a modification in the vicinity of the interface and not taken into account in the Frössling model is responsible for this overestimation. This modification can be hydrodynamic but may also be physicochemical. In current correlations, the diffusion layer is taken to have the same physicochemical properties as the bulk. It is assumed that, for a very concentrated solution, an accumulation of surfactants needs to be taken into account, with a different diffusion coefficient and $[O_2]^*$. Finally, these results highlight the importance of creating a reliable, exact model, and give some clues about the mechanism, because mass transfer is strongly dependent on the length of the hydrophobic tail and the equilibrium adsorption.

4. Conclusion

In this work, the impact of the nature of the surfactants used on oxygen mass transfer has been experimentally measured with the PLIF-I technique. A description of the surface contamination has been given for each system studied and this reveals that the hydrophobic tail of cationic surfactant has an impact on the adsorption isotherm. The longer the chain, the more it adsorbs for low concentrations. In contrast, changing the length of a nonionic surfactant does not significantly affect the adsorption isotherm. Concerning oxygen transfer in liquids containing these surfactants, for every case studied, an increase of the bulk concentration led to a sharp decrease of velocity and mass transfer coefficient. The results suggest that these decreases with increasing concentration of surfactant are strongly related to the adsorption of surfactants on the interface. Concerning the nature of surfactants, if the hydrophobic chain of a cationic surfactant is lengthened, at the same bulk concentration, then the mass transfer coefficient is strongly impacted and is lower for the cases studied here. In contrast, increasing the length of the hydrophilic part of a nonionic surfactant does not have any effect on mass transfer at the same bulk concentration, even if the density of matter at the interface predicted by the Langmuir model is different. Finally, results have been compared with current correlations and show that, for a highly contaminated bubble, the Frössling model overestimates the mass transfer coefficient. These results underline the necessity to create an adapted model that takes account of the adsorption of surfactants at the interface and the resulting changes in physicochemical parameters.

Acknowledgments

The authors wish to thank the French National Research Agency (ANR) for the support from the project MAMOTHS ANR-17-CE06-001 and Bilal El Mokdad for his kind help.

References

[1] Roustan, M., 2003, *Transferts gaz-liquide dans les procédés de traitement des eaux et des effluents gazeux*, Tec & Doc Lavoisier.

[2] Charpentier, J.-C., 1978, “Considérations générales sur les contacteurs gaz-liquide Problèmes fondamentaux et appliqués de métrologie qui se posent. Place de nos recherches,” La Houille Blanche, (5), pp. 315–317.

[3] Treybal, R. E., 1955, *Mass-transfer Operations*. Chemical Engineering series. McGraw-Hill.
[4] Green, D. W., Perry R.H., 2007, *Perry's Chemical Engineers' Handbook, 8th edition*. McGraw-Hill Professional, 2007.
[5] Bouaifi, M., Hebrard, G., Bastoul, D., and Roustan, M., 2001, "A Comparative Study of Gas Hold-up, Bubble Size, Interfacial Area and Mass Transfer Coefficients in Stirred Gas–Liquid Reactors and Bubble Columns," Chemical Engineering and Processing: Process Intensification, **40**(2), pp. 97–111.
[6] Cockx, A., Roustan, M., Line, A., and Hébrard, G., 1995, "Modeling of Mass-Transfer Coefficient K-L in Bubble-Columns," Chemical Engineering Research and Design, **73**(6), pp. 627–631.
[7] Billet, R., and Schultes, M., 1993, "Predicting Mass Transfer in Packed Columns," Chemical Engineering & Technology, **16**, pp. 1–9.
[8] Albal, R. S., Shah, Y. T., Schumpe, A., and Carr, N. L., 1983, "Mass Transfer in Multiphase Agitated Contactors," The Chemical Engineering Journal, **27**(2), pp. 61–80.
[9] Besagni, G., and Inzoli, F., 2017, "The Effect of Liquid Phase Properties on Bubble Column Fluid Dynamics: Gas Holdup, Flow Regime Transition, Bubble Size Distributions and Shapes, Interfacial Areas and Foaming Phenomena," Chemical Engineering Science, **170**, pp. 270–296.
[10] Xu, F., Cockx, A., Hébrard, G., and Dietrich, N., 2018, "Mass Transfer and Diffusion of a Single Bubble Rising in Polymer Solutions," Industrial & Engineering Chemistry Research, **57**(44), pp. 15181–15194.
[11] Duran, C., Fayolle, Y., Pechaud, Y., Cockx, A., and Gillot, S., 2016, "Impact of the Activated Sludge Suspended Solids on Its Non-Newtonian Behavior and Oxygen Transfer in a Bubble Column." Chemical Engineering Science. **141**, pp.154-165.
[12] Lebrun, G., Xu, F., Le Men, C., Hébrard, G., and Dietrich, N., 2021, "Gas–Liquid Mass Transfer around a Rising Bubble: Combined Effect of Rheology and Surfactant," Fluids, **6**(2), p. 84.
[13] Kováts, P., Thévenin, D., and Zähringer, K., 2020, "Influence of Viscosity and Surface Tension on Bubble Dynamics and Mass Transfer in a Model Bubble Column," International Journal of Multiphase Flow, **123**, p. 103174.
[14] García-Abuín, A., Gómez-Díaz, D., Losada, M., and Navaza, J. M., 2013, "Oxygen Absorption in Polymer+surfactant Aqueous Solutions," Chemical Engineering Journal, **225**, pp. 76–83.
[15] Dumont, E., and Delmas, H., 2003, "Mass Transfer Enhancement of Gas Absorption in Oil-in-Water Systems: A Review," Chemical Engineering and Processing: Process Intensification, **42**(6), pp. 419–438.
[16] Nekoeian, S., Aghajani, M., Alavi, S. M., and Sotoudeh, F., 2019, "Effect of Surfactants on Mass Transfer Coefficients in Bubble Column Contactors: An Interpretative Critical Review Study," Reviews in Chemical Engineering, p. 20180089.
[17] Rosso, D., Huo, D. L., and Stenstrom, M. K., 2006, "Effects of Interfacial Surfactant Contamination on Bubble Gas Transfer," Chemical Engineering Science, **61**(16), pp. 5500–5514.
[18] Alves, S. S., Orvalho, S. P., and Vasconcelos, J. M. T., 2005, "Effect of Bubble Contamination on Rise Velocity and Mass Transfer," Chemical Engineering Science, **60**(1), pp. 1–9.
[19] Griffith, R. M., 1962, "The Effect of Surfactants on the Terminal Velocity of Drops and Bubbles," Chemical Engineering Science, **17**(12), pp. 1057–1070.
[20] Weber, M. E., 1975, "The Effect of Surface Active Agents on Mass Transfer from Spherical Cap Bubbles," Chemical Engineering Science, **30**(12), pp. 1507–1510.
[21] Vasconcelos, J. M. T., Orvalho, S. P., and Alves, S. S., 2002, "Gas–Liquid Mass Transfer to Single Bubbles: Effect of Surface Contamination," American Institute of Chemical Engineers Journal, **48**(6), pp. 1145–1154.
[22] Weiner, A., Timmermann, J., Pesci, C., Grewe, J., Hoffmann, M., Schlüter, M., and Bothe, D., 2019, "Experimental and Numerical Investigation of Reactive Species Transport around a Small Rising Bubble," Chemical Engineering Science: X, **1**, p. 100007.
[23] Painmanakul, P., and Hébrard, G., 2008, "Effect of Different Contaminants on the α-Factor: Local Experimental Method and Modeling," Chemical Engineering Research and Design, **86**(11), pp. 1207–1215.

[24] Jimenez, M., Dietrich, N., Grace, J. R., and Hébrard, G., 2014, "Oxygen Mass Transfer and Hydrodynamic Behaviour in Wastewater: Determination of Local Impact of Surfactants by Visualization Techniques," Water Research, **58**, pp. 111–121.
[25] Ahmia, A. C., Idouhar, M., Wongwailikit, K., Dietrich, N., and Hébrard, G., 2019, "Impact of Cellulose and Surfactants on Mass Transfer of Bubble Columns," Chemical Engineering & Technology, **42**(11), pp. 2465–2475.
[26] Gómez-Díaz, D., M. Navaza, J., and Sanjurjo, B., 2009, "Mass-Transfer Enhancement or Reduction by Surfactant Presence at a Gas−Liquid Interface," Industrial & Engineering Chemistry Research, **48**(5), pp. 2671-2677.
[27] Álvarez, E., Gómez-Díaz, D., Navaza, J. M., and Sanjurjo, B., 2008, "Continuous Removal of Carbon Dioxide by Absorption Employing a Bubble Column," Chemical Engineering Journal, **137**(2), pp. 251–256.
[28] Painmanakul, P., Loubière, K., Hébrard, G., Mietton-Peuchot, M., and Roustan, M., 2005, "Effect of Surfactants on Liquid-Side Mass Transfer Coefficients," Chemical Engineering Science, **60**(22), pp. 6480–6491.
[29] Sardeing, R., Painmanakul, P., and Hébrard, G., 2006, "Effect of Surfactants on Liquid-Side Mass Transfer Coefficients in Gas–Liquid Systems: A First Step to Modeling," Chemical Engineering Science, **61**(19), pp. 6249–6260.
[30] Moraveji, M. K., Mohsenzadeh, E., Fakhari, M. E., and Davarnejad, R., 2012, "Effects of Surface Active Agents on Hydrodynamics and Mass Transfer Characteristics in a Split-Cylinder Airlift Bioreactor with Packed Bed," Chemical Engineering Research and Design, **90**(7), pp. 899–905.
[31] Caskey, J. A., and Barlage, W. B., 1972, "A Study of the Effects of Soluble Surfactants on Gas Absorption Using Liquid Laminar Jets," Journal of Colloid and Interface Science, **41**(1), pp. 52–62.
[32] Chen, X., Liu, G., Fan, H., Li, M., Luo, T., Qi, L., and Wang, H., 2013, "Effects of Surfactant Contamination on Oxygen Mass Transfer in Fine Bubble Aeration Process," Korean Journal of Chemical Engineering, **30**(9), pp. 1741–1746.
[33] Jia, X., Hu, W., Yuan, X., and Yu, K., 2015, "Effect of Surfactant Type on Interfacial Area and Liquid Mass Transfer for CO2 Absorption in a Bubble Column," Chinese Journal of Chemical Engineering, **23**(3), pp. 476–481.
[34] Kouzbour, S., Gourich, B., Stiriba, Y., Vial, C., Gros, F., and Sotudeh-Gharebagh, R., 2021, "Experimental Analysis of the Effects of Liquid Phase Surface Tension on the Hydrodynamics and Mass Transfer in a Square Bubble Column," International Journal of Heat and Mass Transfer, **170**, p. 121009.
[35] García-Abuín, A., Gómez-Díaz, D., Navaza, J. M., and Sanjurjo, B., 2010, "Effect of Surfactant Nature upon Absorption in a Bubble Column," Chemical Engineering Science, **65**(15), pp. 4484–4490.
[36] Pesci, C., Weiner, A., Marschall, H., and Bothe, D., 2018, "Computational Analysis of Single Rising Bubbles Influenced by Soluble Surfactant," Journal of Fluid Mechanics, **856**, pp. 709–763.
[37] Deising, D., Bothe, D., and Marschall, H., 2018, "Direct Numerical Simulation of Mass Transfer in Bubbly Flows," Computers & Fluids, **172**, pp. 524–537.
[38] Valiorgue, P., Souzy, N., Hajem, M. E., Hadid, H. B., and Simoëns, S., 2013, "Concentration Measurement in the Wake of a Free Rising Bubble Using Planar Laser-Induced Fluorescence (PLIF) with a Calibration Taking into Account Fluorescence Extinction Variations", Experiments in Fluids, **54**(4), p. 1501.
[39] Stöhr, M., Schanze, J., and Khalili, A., 2009, "Visualization of Gas–Liquid Mass Transfer and Wake Structure of Rising Bubbles Using PH-Sensitive PLIF," Experiments in Fluids, **47**(1), pp. 135–143.
[40] Kong, G., Buist, K. A., Peters, E. A. J. F., and Kuipers, J. A. M., 2018, "Dual Emission LIF Technique for PH and Concentration Field Measurement around a Rising Bubble," Experimental Thermal and Fluid Science, **93**, pp. 186–194.

[41] Hiby, J. W., Braun, D., and Eickel, K. H., 1967, “Eine Fluoreszenzmethode Zur Untersuchung Des Stoffübergangs Bei Der Gasabsorption Im Rieselfilm,” Chemie Ingenieur Technik, **39**(5–6), pp. 297–301.
[42] Someya, S., Bando, S., Song, Y., Chen, B., and Nishio, M., 2005, “DeLIF Measurement of PH Distribution around Dissolving CO2 Droplet in High Pressure Vessel,” International Journal of Heat and Mass Transfer, **48**(12), pp. 2508–2515.
[43] Huang, J., and Saito, T., 2017, “Influences of Gas–Liquid Interface Contamination on Bubble Motions, Bubble Wakes, and Instantaneous Mass Transfer,” Chemical Engineering Science, **157**, pp. 182–199.
[44] Lacassagne, T., Simoëns, S., El Hajem, M., and Champagne, J.-Y., 2018, “Ratiometric, Single-Dye, PH-Sensitive Inhibited Laser-Induced Fluorescence for the Characterization of Mixing and Mass Transfer,” Experiments in Fluids, **59**(1), p. 21.
[45] Wolff, L. M., Liu, Z.-C., and Hanratty, T. J., 1991, “A Fluorescence Technique to Measure Concentration Gradients near an Interface,” American Society of Civil Engineers, pp. 210–218.
[46] Wolff, L. M., and Hanratty, T. J., 1994, “Instantaneous Concentration Profiles of Oxygen Accompanying Absorption in a Stratified Flow,” Experiments in Fluids, **16**(6), pp. 385–392.
[47] Woodrow, P. T., and Duke, S. R., 2001, “Laser-Induced Fluorescence Studies of Oxygen Transfer Across Unsheared Flat and Wavy Air−Water Interfaces,” Industrial & Engineering Chemical Research, **40**(8), pp. 1985–1995.
[48] Butler, C., Lalanne, B., Sandmann, K., Cid, E., and Billet, A.-M., 2018, “Mass Transfer in Taylor Flow: Transfer Rate Modelling from Measurements at the Slug and Film Scale,” International Journal of Multiphase Flow, **105**, pp. 185–201.
[49] Butler, C., Cid, E., and Billet, A.-M., 2016, “Modelling of Mass Transfer in Taylor Flow: Investigation with the PLIF-I Technique,” Chemical Engineering Research and Design, **115,** Part B, pp. 292–302.
[50] Roudet, M., Billet, A.-M., Cazin, S., Risso, F., and Roig, V., 2017, “Experimental Investigation of Interfacial Mass Transfer Mechanisms for a Confined High-Reynolds-Number Bubble Rising in a Thin Gap,” American Institute of Chemical Engineers Journal, **63**(6), pp. 2394–2408.
[51] Roudet, M., Loubiere, K., Gourdon, C., and Cabassud, M., 2011, “Hydrodynamic and Mass Transfer in Inertial Gas–Liquid Flow Regimes through Straight and Meandering Millimetric Square Channels,” Chemical Engineering Science, **66**(13), pp. 2974–2990.
[52] Francois, J., Dietrich, N., Guiraud, P., and Cockx, A., 2011, “Direct Measurement of Mass Transfer around a Single Bubble by Micro-PLIFI,” Chemical Engineering Science, **66**(14), pp. 3328–3338.
[53] Bork, O., Schlueter, M., and Raebiger, N., 2005, “The Impact of Local Phenomena on Mass Transfer in Gas-Liquid Systems,” The Canadian Journal of Chemical Engineering, **83**(4), pp. 658–666.
[54] Stern, O., and Volmer, M., 1919, “Uber die Abklingzeit der Fluoreszenz,” Zeitschrift für Physik, **20**, pp. 183–188.
[55] Jimenez, M., Dietrich, N., and Hébrard, G., 2013, “Mass Transfer in the Wake of Non-Spherical Air Bubbles Quantified by Quenching of Fluorescence,” Chemical Engineering Science, **100**, pp. 160–171.
[56] Dietrich, N., Francois, J., Jimenez, M., Cockx, A., Guiraud, P., and Hébrard, G., 2015, “Fast Measurements of the Gas-Liquid Diffusion Coefficient in the Gaussian Wake of a Spherical Bubble,” Chemical Engineering & Technology, **38**(5), pp. 941–946.
[57] Xu, F., Jimenez, M., Dietrich, N., and Hébrard, G., 2017, “Fast Determination of Gas-Liquid Diffusion Coefficient by an Innovative Double Approach,” Chemical Engineering Science, **170**, pp. 68-76.
[58] Gibbs, J. W. A. of A. and S., 1874, “On the Equilibrium of Heterogeneous Substances,” Transaction of the Connecticut Academy of Art and Science, **3**(2).
[59] Langmuir, I., 1917, “The Constitution and Fundamental Properties of Solids and Liquids” Journal of the American Chemical Society, **39**(9), pp. 1848–1906.
[60] Frumkin, A., 1925, “Die Kapillarkurve Der Höheren Fettsäuren Und Die Zustandsgleichung Der Oberflächenschicht,” Zeitschrift für Physikalische Chemie, **116U**(1), pp. 466–484.

[61] Davies, J. T., 1957, "A Quantitative Kinetic Theory of Emulsion Type, I. Physical Chemistry of the Emulsifying Agent, Gas/Liquid and Liquid/Liquid Interface" Proceeding of the 2nd International Congress of Surface Activity, pp. 426-438.
[62] Tadmouri, R., Zedde, C., Routaboul, C., Micheau, J.-C., and Pimienta, V., 2008, "Partition and Water/Oil Adsorption of Some Surfactants," Journal of Physical Chemistry B, **112**(39), pp. 12318–12325.
[63] Bergeron, V., 1997, "Disjoining Pressures and Film Stability of Alkyltrimethylammonium Bromide Foam Films," Langmuir, **13**(13), pp. 3474–3482.
[64] Gilányi, T., Varga, I., Stubenrauch, C., and Mészáros, R., 2008, "Adsorption of Alkyl Trimethylammonium Bromides at the Air/Water Interface," Journal of Colloid and Interface Science, **317**(2), pp. 395–401.
[65] Palaparthi, R., Papageorgiou, D. T., and Maldarelli, C., 2006, "Theory and Experiments on the Stagnant Cap Regime in the Motion of Spherical Surfactant-Laden Bubbles," Journal of Fluid Mechanics, **559**, p. 1.
[66] Krzan, M., Lunkenheimer, K., and Malysa, K., 2004, "On the Influence of surfactant's polar group on the local and terminal velocities of bubbles", Colloids and Surfaces A: Physicochemical and Engineering Aspects, **250**(1), pp. 431-441.
[67] Higbie, R., 1935, "The Rate of Absorption of a Pure Gas into Still Liquid during Short Periods of Exposure", Transaction of the Institution of Chemical Engineers, **35**(1), pp. 36-60.
[68] Frössling, N., 1938, "Uber Die Verdunstung Fallender Tropfen," Beitr. Geophys. Gerlands, **52**, pp. 170–216.
[69] Clift, R., R Grace, J., and E Weber, M., 1978, *Bubbles, Drops, and Particles*. American Press, New York.
[70] Jimenez M., 2013, *Etude du transfert de matière gaz/liquid en milieu complexes : quantification du transfert d'oxygène par techniques optiques*. INSA, Toulouse.

Supplementary material

Table 4: Details on calculated parameters of bubbles generated in C8TAC solutions

C8TAC					
Concentration (mol/L)	5.1×10^{-3}	2.5×10^{-3}	2.5×10^{-4}	2.5×10^{-5}	4.8×10^{-6}
Bubble velocity (10^{-3} m/s)	139±2	184±3	255±7	263±7	284±8
Bubble diameter (10^{-3} m)	0.97±0.02	0.99±0.02	0.99±0.02	0.98±0.02	1.06±0.02
Equilibrium surface tension (10^{-3}	68±1	69±1	70±1	71±1	71±1

N/m)					
Integral of oxygen concentration field (10^{-5} mg/m)	1.69±0.2	3.51±0.07	4.68±0.1	4.41±0.03	6.10±0.29
Oxygen diffusion coefficient (10^{-9} m^2/s)	1.9±0.3	1.9±0.1	1.95±0.03	1.89±0.06	2.0±0.1
Mass transfer coefficient (10^{-4} m/s)	0.85±0.05	2.3±0.1	4.2±0.3	4.2±0.3	5.4±0.3
Relative standard deviation of mass transfer coefficient	0.12	0.02	0.05	0.01	0.06
Schmidt number	530±90	520±40	513±8	530±20	510±30
Reynolds number	138±4	182±5	252±9	257±9	300±10
Sherwood number	44±10	119±10	210±10	220±10	290±20

Table 5: Details on calculated parameters of bubbles generated in C12TAC solution

C12TAC							
Concentration (mol/L)	1.3×10^{-3}	2.5×10^{-4}	5×10^{-5}	2.5×10^{-5}	2.5×10^{-6}	2.5×10^{-7}	2.5×10^{-8}
Bubble velocity (10^{-3} m/s)	75±1	95±1	183±3	225±2	174±3	192±4	270±8
Bubble diameter (10^{-3} m)	1.06±0.03	1.04±0.03	1.06±0.03	1.07±0.03	1.00±0.02	0.94±0.03	1.01±0.02
Equilibrium surface tension (10^{-3} N/m)	44±1	63±1	70±1	70±1	71±1	70±1	71±1
Integral of oxygen concentration field (10^{-5} mg/m)	1.81±0.1	2.63±0.07	4.7±0.3	5.7±0.1	5.5±0.2	4.6±0.1	5.8±0.4
Oxygen diffusion coefficient (10^{-9} m^2/s)	1.8±0.1	1.9±0.2	1.8±0.1	1.9±0.1	2.0±0.1	1.9±0.1	1.9±0.1
Mass transfer coefficient (10^{-4} m/s)	0.4±0.02	0.81±0.02	2.65±0.2	3.9±0.2	3.3±0.2	3.5±0.2	5.6±0.4
Relative standard deviation of mass transfer coefficient	0.09	0.04	0.08	0.03	0.003	0.02	0.07
Schmidt number	550±20	540±60	550±30	520±20	500±30	520±40	530±20
Reynolds number	79±2	100±3	195±6	241±4	174±5	181±6	272±8
Sherwood number	25±2	45±6	155±14	216±7	168±10	170±20	310±30

Table 6: Details on calculated parameters of bubbles generated in C16TAC solutions

C16TAC							
Concentration (mol/L)	2.5×10^{-3}	2.5×10^{-4}	5×10^{-5}	2.5×10^{-5}	2.5×10^{-6}	2.5×10^{-7}	2.5×10^{-8}
Bubble velocity (10^{-3} m/s)	107±1	125±2	122±2	119±1	132±2	179±3	279±8
Bubble diameter (10^{-3} m)	0.86±0.02	1.08±0.02	0.94±0.02	1.06±0.02	1.00±0.02	0.96±0.02	1.04±0.02
Equilibrium surface tension (10^{-3} N/m)	42±1	51±1	67±1	69±1	70±1	70±1	70±1
Integral of oxygen concentration field (10^{-5} mg/m)	1.37±0.07	1.6±0.1	1.66±0.05	1.9±0.1	2.1±0.1	3.9±0.1	5.6±0.2
Oxygen diffusion coefficient (10^{-9} m^2/s)	1.9±0.2	2.0±0.3	1.9±0.2	2.0±0.2	1.9±0.2	2.0±0.2	2.0±0.1
Mass transfer coefficient (10^{-4} m/s)	0.64±0.04	0.55±0.03	0.77±0.04	0.70±0.04	0.95±0.07	2.5±0.2	5.1±0.3
Relative standard deviation of mass transfer coefficient	0.06	0.05	0.03	0.04	0.05	0.04	0.06
Schmidt number	510±50	510±80	520±40	510±50	510±50	500±50	490±30
Reynolds number	92±2	136±3	115±3	126±3	132±3	172±5	289±9
Sherwood number	28±3	30±5	38±4	38±4	49±6	120±20	260±20

Table 7: Details on calculated parameters of bubbles generated in TX100 solutions

TX100								
Concentration (mol/L)	3.7×10^{-4}	3.7×10^{-5}	2.8×10^{-5}	1.9×10^{-5}	9.4×10^{-6}	3.7×10^{-6}	3.7×10^{-7}	3.7×10^{-8}
Bubble velocity (10^{-3} m/s)	103±1	118±1	113±1	114±1	113±1	113±1	239±6	264±7
Bubble diameter (10^{-3} m)	0.85±0.02	0.99±0.02	0.93±0.02	0.94±0.02	0.93±0.02	0.94±0.02	0.94±0.02	0.99±0.02
Equilibrium surface tension (10^{-3} N/m)	32±1	48±1	50±1	52±1	55±1	60±1	67±1	71±1
Integral of oxygen concentration field (10^{-5} mg/m)	1.27±0.06	1.47±0.03	1.73±0.03	1.63±0.07	2.04±0.06	2.9±0.2	4.1±0.2	5.7±0.2
Oxygen diffusion coefficient (10^{-9} m^2/s)	1.8±0.2	1.7±0.3	2.0±0.1	1.9±0.1	1.9±0.2	1.8±0.1	1.9±0.1	2.0±0.1
Mass transfer coefficient (10^{-4} m/s)	0.63±0.04	0.62±0.04	0.79±0.05	0.74±0.05	0.93±0.06	1.29±0.08	3.4±0.2	5.3±0.3
Relative standard deviation of mass transfer coefficient	0.05	0.03	0.05	0.05	0.03	0.05	0.06	0.04
Schmidt number	560±60	600±100	510±40	520±30	530±30	560±30	540±30	500±30
Reynolds number	87±2	117±3	105±2	107±2	105±2	107±2	238±7	261±8
Sherwood number	30±4	37±8	37±3	36±3	46±4	68±6	180±20	260±20

Table 8: Details on calculated parameters of bubbles generated in TX102 solutions

TX102							
Concentration (mol/L)	3.7×10^{-4}	2.8×10^{-5}	1.9×10^{-5}	9.4×10^{-6}	3.7×10^{-6}	3.7×10^{-7}	3.7×10^{-8}
Bubble velocity (10^{-3} m/s)	101±1	110±1	111±1	110±1	113±1	204±4	269±7
Bubble diameter (10^{-3} m)	0.83±0.02	0.93±0.02	0.93±0.02	0.93±0.02	0.93±0.02	0.94±0.02	0.99±0.02
Equilibrium surface tension (10^{-3} N/m)	35±1	50±1	53±1	56±1	60±1	69±1	71±1
Integral of oxygen concentration field (10^{-5} mg/m)	1.22±0.06	1.38±0.08	1.9±0.1	2.24±0.06	4.3±0.1	4.2±0.1	5.51±0.24
Oxygen diffusion coefficient (10^{-9} m^2/s)	1.9±0.1	1.9±0.1	1.9±0.1	1.9±0.1	1.8±0.1	1.84±0.04	2.0±0.1
Mass transfer coefficient (10^{-4} m/s)	0.63±0.04	0.61±0.04	0.84±0.04	1.00±0.05	1.9±0.1	3.3±0.2	5.5±0.3
Relative standard deviation of mass transfer coefficient	0.05	0.07	0.05	0.05	0.03	0.03	0.04
Schmidt number	530±30	530±40	530±50	520±20	550±50	540±10	500±30
Reynolds number	83±2	103±2	103±2	103±2	105±2	192±5	266±9
Sherwood number	28±2	30±3	42±5	48±3	98±9	170±9	270±20

Table 9: Details on calculated parameters of bubbles generated in TX165 solutions

TX165								
Concentration (mol/L)	3.7×10^{-4}	3.7×10^{-5}	2.8×10^{-5}	1.9×10^{-5}	9.4×10^{-6}	3.7×10^{-6}	3.7×10^{-7}	3.7×10^{-8}
Bubble velocity (10^{-3} m/s)	99±1	112±1	118±1	118±1	118±1	111±1	199±4	224±5
Bubble diameter (10^{-3} m)	0.82±0.02	0.93±0.02	0.95±0.02	1.01±0.02	1.00±0.02	0.94±0.02	0.94±0.02	0.92±0.02
Equilibrium surface tension (10^{-3} N/m)	41±1	53±1	55±1	56±1	58±1	62±1	67±1	70±1
Integral of oxygen concentration field (10^{-5} mg/m)	1.49±0.04	1.6±0.1	1.76±0.08	1.85±0.1	2.28±0.06	3.4±0.1	4.3±0.1	5.9±0.1
Oxygen diffusion coefficient (10^{-9} m^2/s)	1.8±0.1	2.0±0.2	1.8±0.1	1.83±0.05	1.9±0.1	1.88±0.07	1.91±0.06	1.92±0.07
Mass transfer coefficient (10^{-4} m/s)	0.74±0.02	0.74±0.04	0.75±0.04	0.77±0.04	0.96±0.06	1.52±0.09	3.5±0.2	5.5±0.3
Relative standard deviation of mass transfer coefficient	0.03	0.07	0.04	0.05	0.05	0.05	0.03	0.01
Schmidt number	540±40	510±50	560±30	550±20	540±30	530±20	520±20	520±20
Reynolds number	82±2	104±2	117±3	119±3	118±3	104±2	186±5	207±6
Sherwood number	33±3	35±4	41±3	42±3	51±4	76±5	170±10	260±20

Table 10: Details on calculated parameters of bubbles generated in TX100 solutions

TX305							
Concentration (mol/L)	3.8×10^{-4}	3.8×10^{-5}	2.8×10^{-5}	9.4×10^{-6}	3.7×10^{-6}	3.7×10^{-7}	3.7×10^{-8}
Bubble velocity (10^{-3} m/s)	100±1	117±1	119±1	117±1	127±2	216±5	283±8
Bubble diameter (10^{-3} m)	0.86±0.02	0.97±0.02	0.98±0.02	1.00±0.02	1.07±0.02	1.06±0.02	1.05±0.02
Equilibrium surface tension (10^{-3} N/m)	47±1	57±1	58±1	59±1	60±1	64±1	69±1
Integral of oxygen concentration field (10^{-5} mg/m)	1.79±0.08	1.74±0.03	1.7±0.1	1.70±0.07	3.3±0.1	4.62±0.48	5.5±0.1
Oxygen diffusion coefficient (10^{-9} m^2/s)	2.0±0.2	1.9±0.2	1.93±0.08	1.9±0.1	1.88±0.07	1.9±0.1	1.92±0.08
Mass transfer coefficient (10^{-4} m/s)	0.87±0.05	0.77±0.04	0.75±0.04	0.71±0.04	1.30±0.07	3.1±0.2	5.0±0.3
Relative standard deviation of mass transfer coefficient	0.05	0.01	0.05	0.04	0.04	0.03	0.02
Schmidt number	500±50	530±50	520±20	530±30	530±20	520±30	520±20
Reynolds number	85±2	114±3	117±3	117±3	136±3	229±6	300±10
Sherwood number	37±2	39±2	38±2	37±2	74±4	170±20	270±20

Graphical abstract